Comparative fatigue performance of as-built vs etched Ti64 in TPMS-gyroid and stochastic structures fabricated via PBF-LB for biomedical applications

Miguel Araya-Calvo
Bio-inspired Processes and Materials Research Group, Tecnologico de Costa Rica, Cartago, Costa Rica and
Future Manufacturing Technologies Research Group, Kerttu Saalasti Institute, University of Oulu, Oulu, Finland

Antti Järvenpää and Timo Rautio
Future Manufacturing Technologies Research Group, Kerttu Saalasti Institute, University of Oulu, Oulu, Finland

Johan Enrique Morales-Sanchez
Biology Department, Tecnologico de Costa Rica, Cartago, Costa Rica, and

Teodolito Guillen-Girón
Bio-inspired Processes and Materials Research Group, Tecnologico de Costa Rica, Cartago, Costa Rica

Abstract

Purpose – This study compares the fatigue performance and biocompatibility of as-built and chemically etched Ti-6Al-4V alloys in TPMS-gyroid and stochastic structures fabricated via Powder Bed Fusion Laser Beam (PBF-LB). This study aims to understand how complex lattice structures and post-manufacturing treatment, particularly chemical etching, affect the mechanical properties, surface morphology, fatigue resistance and biocompatibility of these metamaterials for biomedical applications.

Design/methodology/approach – Selective Laser Melting (SLM) technology was used to fabricate TPMS-gyroid and Voronoi stochastic designs with three different relative densities (0.2, 0.3 and 0.4) in Ti-6Al-4V ELI alloy. The as-built samples underwent a chemical etching process to enhance surface quality. Mechanical characterization included static compression and dynamic fatigue testing, complemented by scanning electron microscopy (SEM) for surface and failure analysis. The biocompatibility of the samples was assessed through *in-vitro* cell viability assays using the Alamar Blue assay and cell proliferation studies.

Findings – Chemical etching significantly improves the surface morphology, mechanical properties and fatigue resistance of both TPMS-gyroid and stochastic structures. Gyroid structures demonstrated superior mechanical performance and fatigue resistance compared to stochastic structures, with etching providing more pronounced benefits in these aspects. *In-vitro* biocompatibility tests showed high cytocompatibility for both as-built and etched samples, with etched samples exhibiting notably improved cell viability. The study also highlights the importance of design and post-processing in optimizing the performance of Ti64 components for biomedical applications.

Originality/value – The comparative analysis between as-built and etched conditions, alongside considering different lattice designs, provides valuable information for developing advanced biomedical implants. The demonstration of enhanced fatigue resistance and biocompatibility through etching adds significant value to the field of additive manufacturing, suggesting new avenues for designing and post-processing implantable devices.

Keywords Fatigue, Additive manufacturing, Powder bed fusion laser beam

Paper type Research paper

1. Introduction

The Ti6-Al-4V (Ti64) alloy stands out as a material of choice for medical implants that bear loads owing to its excellent biocompatibility, superior mechanical strength and enhanced corrosion resistance. These attributes have rendered it a popular material in the medical field, providing optimal functionality and patient safety (Ataee *et al.*, 2018; Bartolomeu *et al.*, 2021;

The current issue and full text archive of this journal is available on Emerald Insight at: **https://www.emerald.com/insight/1355-2546.htm**

Rapid Prototyping Journal
30/11 (2024) 216–229
Emerald Publishing Limited [ISSN 1355-2546]
[DOI 10.1108/RPJ-04-2024-0152]

The authors gratefully acknowledge the Future Manufacturing Technologies (FMT) research group at the Kerttu Saalasti Institute, University of Oulu, and the Research Vicerrectory of Tecnológico de Costa Rica for funding the experimental work. Authors also appreciate Business Finland for supporting the DREAMS project and the Finnish National Agency for Education (EDUFI) for the scholarship that enabled this international collaboration. Additionally, we acknowledge the Industrial Design Engineering School at Tecnológico de Costa Rica for supporting the publication of this work.

Funding: Business Finland DREAMS project; 4795/31/2021.

Received 3 April 2024
Revised 23 May 2024
Accepted 22 July 2024

Murr *et al.*, 2011; Soro *et al.*, 2022; Yang *et al.*, 2019). However, despite its advantageous properties, the inherent stiffness of this alloy in its solid form creates a disparity with the natural bone, leading to stress shielding. This mismatch can precipitate bone resorption as the bone remodels in response to stress, undermining the implant's durability and efficacy (Ataee *et al.*, 2018; Yan *et al.*, 2019). The challenge is further compounded by the significant difference in the elastic modulus between the Ti6Al4V alloy and bone tissues, necessitating materials that offer both robustness and a modulus that more closely aligns with that of bone tissue (Yan *et al.*, 2019).

To address this challenge, porous biomaterials emerge as a viable solution, especially in tissue engineering and orthopedic implants. Their use not only provides mechanical support and fatigue resistance but also mitigates the risk of stress shielding (Bobbert *et al.*, 2017; Jam *et al.*, 2022; Mondal *et al.*, 2022).

Additive manufacturing (AM) plays a pivotal role in the advancement of these materials, allowing the creation of components with complex geometries that traditional methods cannot achieve, including porous metallic lattices, with many beneficial mechanical and biological properties in the manufacture of biomedical devices (Cao *et al.*, 2022; Evans *et al.*, 2018; Huang *et al.*, 2023; Oosterbeek *et al.*, 2023). Powder Bed Fusion Laser Beam (PBF-LB) techniques have gained attention for their ability to fabricate detailed internal structures, including those with small strut sizes. This capability aligns well with the requirements for bone tissue engineering, where a specific pore size range is crucial for successful integration with bone (Barba *et al.*, 2019; Choy *et al.*, 2017; Soro *et al.*, 2022; Tyagi and Manjaiah, 2023; Wu *et al.*, 2023).

Among various PBF-LB technologies, Selective Laser Melting (SLM) shows significant promise. This method facilitates the layer-by-layer fusion of metallic powder using a high-energy laser beam, enabling the production of cellular structures from Ti6Al4V that exhibit an elastic modulus comparable to bone tissue. These structures not only hold potential for orthopedic applications but also highlight the viability of using SLM for manufacturing implants that can better mimic the mechanical properties of bone (Bartolomeu *et al.*, 2021; Dhiman *et al.*, 2019; Huang *et al.*, 2020; Kumawat *et al.*, 2023; Ma *et al.*, 2020; Yan *et al.*, 2019).

The impact of characteristics inherent to cellular solids, including porosity, size and shape of structural units and surface roughness, on their mechanical strength and biocompatibility has undergone thorough examination that underscores the pivotal importance of these attributes in determining the performance of cellular solids and their integration with tissue (Marin, 2023). Lattice structures, with their interconnected struts, present a unique set of mechanical properties and porosity that make them particularly suitable for orthopedic implants and scaffolds (Bandyopadhyay *et al.*, 2023; Kechagias *et al.*, 2022; Tyagi and Manjaiah, 2023). Depending on their microstructure, these lattices can display patterns that are either regular (periodic) or irregular (non-periodic), with the latter often described as stochastic (McGregor *et al.*, 2021; Yu *et al.*, 2022).

Triply periodic minimal surfaces (TPMS) are periodic structures with minimal and extensive surface area properties, offering an even stress distribution under load. Their geometric and mechanical properties make them particularly attractive for biomedical applications, resembling the mean curvature of trabecular bone and mimicking bone tissue properties. The gyroid structure, a type of TPMS, stands out for its potential in high-value engineering applications, particularly in porous bio-implants (Barba *et al.*, 2019; Bobbert *et al.*, 2017; Wu *et al.*, 2023).

While the focus on periodic structures has advanced our understanding of their mechanical behavior, less attention has been paid to stochastic structures despite their relevance in designing parts with irregular geometries or emulating complex natural structures like trabecular bone (Deering and Grandfield, 2021). Nevertheless, efforts are being made in research to develop functionally graded stochastic topologies through additive manufacturing, which more accurately replicate the microstructure of bone (Vyavahare *et al.*, 2023). Using lattice-based Voronoi structures can enhance the functional performance of medical devices when compared to traditional parts in the biomedical field (Bregoli *et al.*, 2024). This highlights the importance of exploring both periodic and non-periodic structures, especially in applications demanding specific porosity and structural integrity to promote bone ingrowth and facilitate tissue regeneration (Ghouse *et al.*, 2018; Kechagias *et al.*, 2022).

Improving the surface condition of additively manufactured Ti-6Al-4V, particularly by chemical etching, significantly enhances its fatigue life. This method is more effective than merely correcting internal defects with heat treatment or leaving surfaces in their as-built state (Sun *et al.*, 2020). Furthermore, the comparative analysis of as-built versus etched Ti64 in both TPMS-gyroid and stochastic structures manufactured via PBF-LB is crucial. This comparison not only sheds light on the fatigue performance of these materials but also explores the influence of surface quality, which is known to impact the cyclic mechanical performance of additively manufactured materials adversely. Given the high surface roughness characteristic of AM materials, understanding how different post-processing techniques affect the mechanical properties of these structures is essential for optimizing their design and application in biomedical implants (Van Hooreweder *et al.*, 2017).

2. Methodology and materials

2.1 Lattices design and manufacturing

The research examined two distinct open-cell lattice configurations: a gyroid structure with walls based on the Triply Periodic Minimal Surface (TPMS), governed by equation (1), where "a" determines the size of the unit cell, while "t" influences its porosity (Zhao *et al.*, 2021). The second configuration explored was a Voronoi Volume Lattice, characterized by its stochastic arrangement formed through random points within space. These configurations represent two of the primary classifications of lattice structures, with the former being shaped by mathematical surfaces and the latter consisting of elements resembling struts or beams (Barba *et al.*, 2019):

$$\theta(x,y,z)_{Gyroid} = \sin\left(\frac{2\pi}{a}x\right)cos\left(\frac{2\pi}{a}y\right) + \sin\left(\frac{2\pi}{a}y\right)cos\left(\frac{2\pi}{a}z\right) + sin\left(\frac{2\pi}{a}z\right)cos\left(\frac{2\pi}{a}x\right) = t \quad (1)$$

The lattice designs were created digitally through implicit modeling techniques using nTopology software based in New York, USA. Implicit modeling was used as a method that

efficiently represents three-dimensional structures with a mathematical function that defines a solid's shape. Three relative densities of 0.2, 0.3 and 0.4 were considered in both structures to study the effect of porosity and design on the compressive properties. The six different models are detailed in Figure 1.

The lattices were constructed with varying thicknesses: wall thickness for the TPMS Gyroid and strut thickness for the Stochastic Voronoi structures to obtain a desired relative density (RD), starting at 225 μm, corresponding to a lower RD of 0.2 and increased by 25 μm up to 275 μm for a higher RD of 0.4, as depicted in Figure 1. Two primary factors were adjusted to achieve the targeted RD for each thickness: the unit cell size for the TPMS Gyroid and the mean distance between random spatial points for the Stochastic Voronoi structures. The design parameters are detailed in Table 1.

Cylindrical compression samples with a diameter of 12 mm were designed, featuring a top and bottom plate, each 1 mm thick and lattice structures of 18 mm in height. Detailed specifications of these samples are shown in Figure 2.

The structures were produced using PBF-LB AM, specifically through Selective Laser Melting (SLM) technology. The SLM 280 HL 3D printer and powdered Ti-6Al-4V ELI (Grade 23) Titanium, supplied by SLM Solutions in Lübeck, Germany, was used. This titanium powder features spherical particles with a diameter of 30 μm and a density of 4.43 g/cm^3. Prior to starting the manufacturing process, the base plate was heated to 200°C. The fabrication was carried out at a theoretical rate of 14.2 cm^3/h, maintaining a uniform layer thickness of 0.03 mm. Hatching

Figure 2 Design specifications of compressive specimens

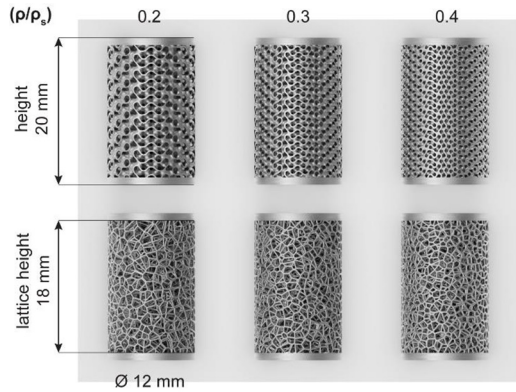

Source: Figure by authors

Figure 1 Set of 6 different models for the present study

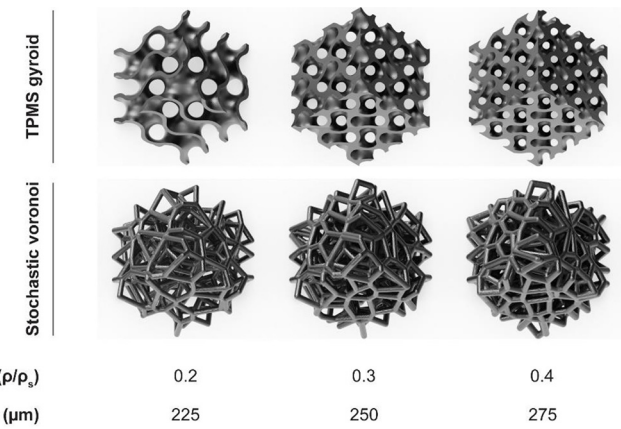

Note: The set comprises 2 lattice structures (walled TPMS gyroid and Stochastic) and 3 different relative densities of 0.2, 0.3 and 0.4
Source: Figure by authors

Table 1 Design parameters for the structures modeling

Structure	Wall/strut thickness (μm)	Unit cell size (mm)	Averaged distance of random points in space (mm)	Lattice volume (mm^3)	Relative density (ρ/ρ_s)
TPMS gyroid	225	2.170	NA	407.200	0.200
	250	1.616	NA	611.688	0.300
	275	1.339	NA	814.443	0.400
Stochastic	225	NA	1.133	407.157	0.200
	250	NA	0.977	611.265	0.300
	275	NA	0.889	815.386	0.400

Source: Created by authors

parameters were adjusted to a tolerance of 0.1 mm and a spacing of 0.12 mm. For the laser settings, 500 watts was used for contours and 300 watts for internal hatches. The fill patterns used included "Stripes" for outer areas and "Chessboard" for the volume core. The samples were positioned randomly on the platform to minimize the impact of fabrication parameters on the outcomes.

2.2 Surface treatment

The samples underwent one of two treatments: the first group of samples was tested as built and subjected to a cleaning procedure only, while the second group was subject to a cleaning and an etching procedure. For both conditions, a Cole Parmer 8892 model ultrasonic cleaner was used. The cleaning regimen involved using the ultrasonic cleaner for two consecutive sessions: initially, for 30 min in 100 mL of distilled water, followed by another 30 min in 100 mL of ethanol. The etching was applied after the cleaning with a mixture of ammonium hydroxide NH_4OH (70%) and hydrogen peroxide H_2O_2 (30%). The settings for the ultrasonic bath during the etching were adjusted to maintain a temperature of 50°C for one hour.

2.3 Mechanical characterization

Compressive static tests were performed with a Tinius Olsen Universal System Machine and a 50KN cell load. The compression strain rate used was 10^{-2} s^{-1} in accordance with the standard ISO 13314 –Mechanical testing of metals – Ductility testing – Compression test for porous and cellular Metals. Each static compression test was related to a stress–strain curve for each structure, from which the following values were calculated: elastic modulus (E_0) and yield strength (σ_y). The test was made with one replicate for a total of 24 samples, two for each combination of variables: structure (Gyroid vs Stochastic), RD (0.2 vs 0.3 vs 0.4) and treatment (as-built vs etching).

After static mechanical evaluation, 0.3 RD structures were selected to evaluate the fatigue response. Fatigue testing was performed with an MTS Bionix Universal System Machine by using a 25KN cell load. All samples were subjected to constant amplitude sinusoidal loading under compression-compression conditions at a steady test frequency of 15 Hz and a fixed load ratio of $R = 0.1$. All tests were conducted under force control, and a stress-based method was used for the fatigue analysis. Amplitude force values were chosen for each porous structure based on each yield strength for 0.1 σ_y and 0.5 σ_y. The dynamic test was made with one replicate for a total of 16 samples, two for each combination of variables: structure (Gyroid vs Stochastic), treatment (as-built vs etching) and force control (0.1 σ_y vs 0.5 σ_y). Each test continued until the failure of the structure or if 10^6 cycles were achieved.

2.4 Scanning electron microscopy

A Scanning Electron Microscopy (SEM) was used to analyze the microstructure of the samples in as-built condition and etching treatment. This analysis was performed to identify and verify the internal structure of the samples, characterize SLM technology, analyze the etching effect and examine the failure mechanism. The specimens were mounted using carbon conducting tape. A Jeol JSM-6010LA SEM was used at 20 kV.

2.5 In-vitro biocompatibility tests

The osteosarcoma cell line SaOS-2 was acquired from the American Type Culture Collection (VA, USA). SaOS-2 cells were chosen as they possess multiple osteoblastic characteristics that mimic the entire differentiation sequence of osteoblastic cells in response to outer stimuli (Pereira *et al.*, 2020). Cells were cultured using McCoy's 5a Medium (GIBCO) supplemented with 15% fetal bovine serum (SIGMA) and 1% penicillin-streptomycin (GIBCO). Cells were incubated at 37°C with 5% CO2 and cultivated until reaching confluence, with periodic media changes. Upon confluence, the cells were detached using 0.25 Trypsin (GIBCO) and then directly seeded onto the surface of the subject specimens.

The biocompatibility was evaluated in accordance with the "Biological assessment of medical devices" ISO 10993–5 standard, with adaptations. The assessment included examining the survival and growth of the SaOS-2 cell line directly seeded onto the specimen's surface after 48 and 72 h.

Before conducting the tests, two Synthetized Laser Melting specimens (as built and with etching) were cleaned with 70° ethanol and distilled water, sterilized by autoclaving at 120°C for 1 h and dried in a sterile atmosphere. The specimens were arranged in a polystyrene 24-well plate, and 500 μL of media containing 3.0x104 or 3.5x104 cells were seeded according to their evaluation time (48 or 72 h respectively). Cultures were incubated in appropriate conditions during the evaluation periods; commercial polystyrene surface wells without specimen with normal medium were used as a positive control and commercial polystyrene surface wells without specimen with 10% DMSO supplemented medium were used as a negative control. After the incubation period, specimens were transferred to a fresh well. Alamar Blue reagent (Invitrogen) was applied for 2 h to both the original well to evaluate cells growing on the surface of the well and the new one to evaluate only the cells growing on the surface of the specimen.

Two separate experiments were conducted for each specimen, and three 100 μL samples of media from each well were used to measure cell viability by obtaining optical density readings at 570 nm. Statistical analysis included calculating the mean value and standard deviation, followed by a comparative t-test analysis. Statistically significant differences between the processed alloy and control values were considered at $p < 0.05$.

3. Results and discussion

3.1 Lattices design and manufacturing

Using the SLM 280 HL printer, samples were successfully created through additive manufacturing. By adjusting the strut thickness between 225 and 375 μm, three different relative densities of 0.2, 0.3 and 0.4 were obtained for both the Gyroid TPMS and Voronoi stochastic designs. Each structure demonstrated the expected geometric features and connectivity throughout the various densities. Figure 3 illustrates the surface morphology of the as-built condition and the etching treatment. Observations included some macro defects associated with manufacturing, notably the staircase effect, voids in the walls/struts and roughness in the surface; all of these are typical in the PBF-LB process due to its layer-by-layer construction approach (Günther *et al.*, 2023). The upper surfaces of the samples featured a contour envelope surface

Figure 3 Etching effect SEM micrographs. As built condition at 100x

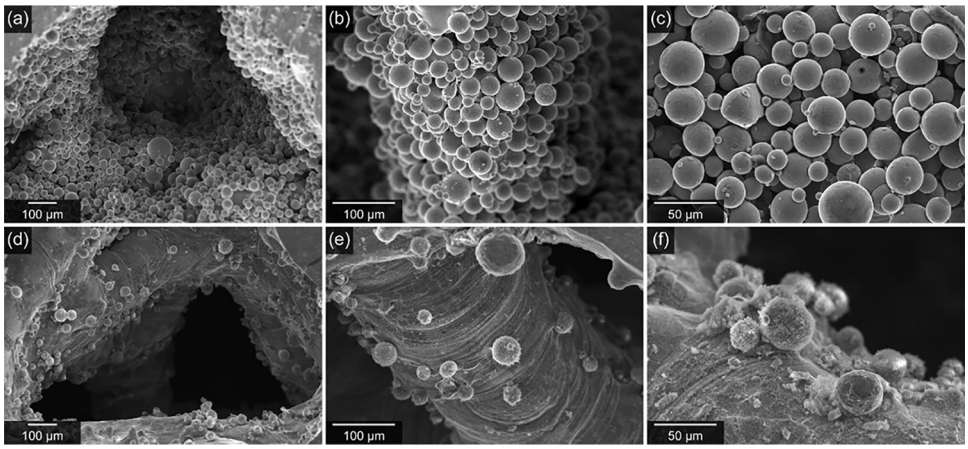

Notes: As built condition at 100x (a); 250x (b) and 500x (c); Etching treatment at 90x (d); 250x (e) and 500x (f)
Source: Figure by authors

marked by numerous slice layers, leading to rough surface textures. This roughness is likely due to the adhesion of partially melted powder particles to the structures' surfaces, compounded by the staircase effect (Sun *et al.*, 2022; Yang *et al.*, 2019). In both structures, unmelted material was noticeable across all relative densities, aligning with findings from earlier studies (Ataee *et al.*, 2018; Kechagias *et al.*, 2022; Sun *et al.*, 2022).

The as-built condition reveals a significantly rough surface on the struts along with visible unmelted powder particles, as depicted in Figure 3 (a)–(c). In contrast, the etched sample displays smoother struts. A smooth surface is expected to enhance the fatigue performance of these biomaterials. The etching process's morphological impacts align with findings from previous investigations (Van Hooreweder *et al.*, 2017; Van Hooreweder and Kruth, 2017; Sun *et al.*, 2020).

3.2 Mechanical characterization

3.2.1 Mechanical behavior under static compressive loading

The mechanical properties of TPMS-Gyroid and Stochastic structures of Ti64 were characterized, focusing on Young's Modulus and Yield Strength under static compressive loading. The structures were analyzed in as-built and etched conditions, with varying relative densities of 0.2, 0.3 and 0.4. The results, summarized in Table 2, reveal significant insights into the mechanical performance of these structures. Figure 4 shows the stress–strain curves of the static test.

The phases of deformation under compression loads depicted in Figure 4 are consistent with experimental results found in existing research (Araya *et al.*, 2024; Gibson, 2005; Hanks *et al.*, 2020; Zhang *et al.*, 2024). These phases include: (i) a linear elastic phase associated with the bending of cell edges or stretching of cell faces; (ii) a stress plateau phase, signaling the progressive failure of cells through elastic buckling and plastic deformation; and (iii) a densification phase, characterized by the complete collapse of the cells and the resulting compression between cell edges and faces. It should be highlighted that gyroid structures with the highest RD exceeded the loading capacity of the testing machine, preventing the specimens from experiencing the stress plateau and densification phases.

As expected, Young's Modulus and Yield Strength increase as the RD increases. For TPMS-Gyroid structures, as-built samples exhibited a progressive rise in Young's Modulus from 2.705 GPa (RD 0.2) to 4.580 GPa (RD 0.2), accompanied by an increase in Yield Strength from 130.424 to 340.072 MPa. The etched samples showed a similar trend, with slight improvements in mechanical properties; for instance, the Young's Modulus increased from 2.810 GPa (RD 0.2) to 4.546 GPa (RD 0.2), and Yield Strength improved from 134.186 to 344.438 MPa. The Stochastic structures followed a similar trend, with mechanical properties increasing alongside RD. However, the as-built Stochastic samples generally exhibited lower Young's Modulus and Yield Strength across all RD levels compared to the TPMS-Gyroid structures. The Young's Modulus ranged from 2.447 GPa (RD 0.2) to 4.361 GPa (RD 0.4), and Yield Strength varied from 111.426 to 259.093 MPa. The etched Stochastic structures showed a decrease in Young's Modulus at RD 0.2 and 0.3 compared to their as-built counterparts but observed improvements in Yield Strength. At RD 0.4, the etched condition yielded a Young's Modulus of 4.140 GPa and Yield Strength of 268.920 MPa, suggesting that etching has a nuanced effect on Stochastic structures, possibly due to their inherent randomness affecting the uniformity of etching benefits.

These results show a lower Young's Modulus but, interestingly, a significantly higher Yield Strength than reported in previous investigations under similar parameters for gyroid (Kelly *et al.*, 2019; Timercan *et al.*, 2023) and stochastic structures (Ghouse *et al.*, 2017; Kechagias *et al.*, 2022). The differences might be related to differences in machine, laser and design related parameters.

Our findings contrast with the reduction or non-effect of mechanical properties presented after chemical etching on Ti64 parts manufactured via PBF-LB when compared with previous investigations (Claros *et al.*, 2016; Surmeneva *et al.*, 2022). The differences might be attributed to differences in the initial structure

Table 2 Compressive characterization

Structure	Treatment	Relative density (ρ/ρ_s)	Young modulus (gpa)	Yield strength (MPa)
TPMS gyroid	As-built	0.200	2.705	130.424
TPMS gyroid	As-built	0.300	3.636	200.650
TPMS gyroid	As-built	0.400	4.580	340.072
TPMS gyroid	Etching	0.200	2.810	134.186
TPMS gyroid	Etching	0.300	3.624	219.346
TPMS gyroid	Etching	0.400	4.546	344.438
Stochastic	As-built	0.200	2.447	111.426
Stochastic	As-built	0.300	3.430	189.424
Stochastic	As-built	0.400	4.361	259.093
Stochastic	Etching	0.200	2.406	117.325
Stochastic	Etching	0.300	3.295	169.812
Stochastic	Etching	0.400	4.140	268.920

Source: Created by authors

Figure 4 Mechanical characterization of SLM specimens.

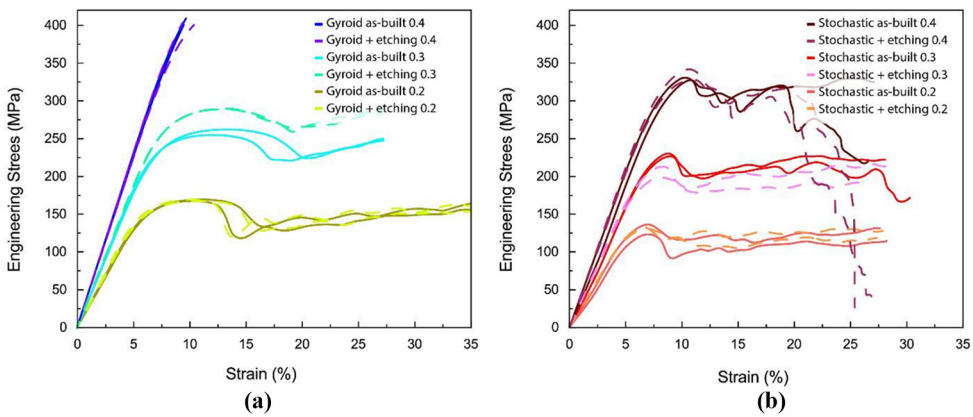

Notes: (a)TPMS Gyroid - Compressive Engineering Stress-Strain; (b)Stochastic Voronoi - Compressive Stress-Strain
Source: Figure by authors

and morphology of different PBF-LB technologies and the etching technique variables (ratio and concentration, aging of the solution, duration and temperature) (Surmeneva *et al.*, 2022).

In addition to relative density, the microarchitecture of the lattice structure also played a role in determining the mechanical properties of latticed structures (Seharing *et al.*, 2020). The comparison between TPMS-Gyroid and Stochastic structures highlights the superior mechanical performance of Gyroid structures, particularly in terms of Young's Modulus and Yield Strength. This could be attributed to the more organized nature of gyroid geometry, which potentially distributes stress more evenly. The etching process generally improves the mechanical properties of both structures, albeit with more pronounced benefits for the Gyroid structures. This improvement is likely due to the reduction of surface flaws and microcracks that can act as stress concentrators, thus enhancing the load-bearing capacity of the material.

3.2.2 Effect of lattice design on compressive behavior

Figure 5 uses the Ashby framework to outline the mechanical properties, illustrating both the elastic modulus and yield stress as they relate to RD (Ashby and Medalist, 1983). Following Ashby's approach, the data have been correlated with linear equations to describe the elastic modulus (E^*) and the strength (σ^*) of the lattice structure, according to equations (2) and (3):

$$\frac{E^*}{E_s} = C_E\left(\frac{\rho^*}{\rho_s}\right)^{m_E} \tag{2}$$

$$\frac{E^*}{E_s} = C_\sigma\left(\frac{\rho^*}{\rho_s}\right)^{m_\sigma} \tag{3}$$

Here, E_s and σ_s denote the elastic modulus and yield strength of solid Ti6Al4V, while C_E, C_σ, m_E and m_σ are constants unique to the lattice design. The values of m_E and m_σ depend on the mode of deformation; for stretch-dominated lattices, m_E and m_σ are set to 1, whereas for bend-dominated ones, the values are $m_E = 2$ and $m_\sigma = 1.5$ (Barba *et al.*, 2019).

Both Gyroid and Stochastic lattices display stretch-dominated behavior in terms of stiffness, with Gyroid structures showing consistently higher stiffness at all levels of relative density

Figure 5 Compressive elastic modulus vs RD Ashby's diagram

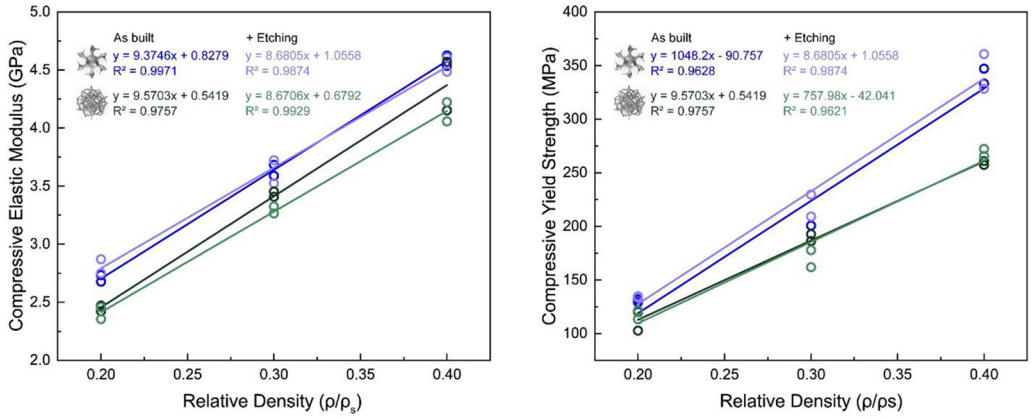

Notes: (a) Compressive Yield Strength vs (b) RD Ashby's diagram
Source: Figure by authors

compared to Stochastic ones. There exists a distinct difference in mechanical strength between the two types of lattices; while Gyroid lattices continue to exhibit stretch-dominated behavior consistent with their stiffness, Stochastic lattices respond to loading with bend-dominated behavior. Gyroid lattice structures offer greater resistance as the relative density increases, compared to their Stochastic counterparts. The chemical etching treatment didn't show any effect on the mode of deformation, which was defined primarily by the type of structure. It is noted that most cellular structures exhibit primarily bend-dominated deformation (Tan *et al.*, 2017).

The observed trends underscore the importance of structural design and post-processing treatments in optimizing the mechanical performance of Ti64 components manufactured via PBF-LB. The increase in mechanical properties with RD suggests a potential strategy for tailoring the strength and stiffness of components to specific application requirements by adjusting the internal architecture.

3.2.3 Mechanical behavior under dynamic c-c loading

Fatigue testing showed different behavior between the two studied structures and the treatment conditions. Figures 6 and 7 show the dynamic results of strain vs cycles and stress vs cycles, respectively.

Both gyroid and stochastic structures demonstrated a more stable strain amplitude across as-built and etched conditions until 10^4 cycles and 10^5 cycles at 0.5 σ_y and 0.1 σ_y, respectively, as shown in Figure 6. Stochastic structures, however, tend to exhibit a broader range of strain responses, indicating a potential for more variability in fatigue performance. This might be related to the randomness of the structure design. Stochastic structures appear to have a lower initial strain amplitude and face earlier failure points than some gyroid structures at 0.5 σ_y, suggesting that stochastic structures may be less resilient to higher stress levels compared to gyroid structures.

Etching treatment seems to improve the fatigue resistance in gyroid structures but more significantly in stochastic structures at 0.1 σ_y, as shown in Figure 6 (d). This is evidenced by a more constant strain amplitude over a longer cycle range before widening.

The material's softening, indicated by an increase in strain amplitude over cycles, is more pronounced in as-built conditions and after 10^4 cycles for all the structures, Hardening behavior, shown by a decrease in strain amplitude, was not prominently observed.

Both structures demonstrate High Cycle Fatigue (HCF) resistance at a lower stress level (0.1 σ_y), with stochastic structures slightly outperforming gyroid structures in maintaining a consistent strain amplitude over 10^5 cycles. Etching tends to slightly improve the HCF resistance in both structures by consistently maintaining or slightly increasing the strain amplitude over cycles. Surface roughness improvements by chemical etching have been reported to enhance latticed structures' fatigue performance (Oosterbeek *et al.*, 2023), also with a combination of hot isostatic pressing (HIP) to provide further improvements to fatigue strength (Ahmadi *et al.*, 2019; Karami *et al.*, 2020).

When tested at a higher stress level (0.5 σ_y), the HCF resistance of both structures decreased. However, gyroid structures appear to have a slightly better resistance to high-cycle fatigue than stochastic structures in both as-built and with etching conditions, potentially due to the uniform distribution of stress and strain throughout the gyroid structure. The geometric regularity of gyroid structures facilitates a more even distribution of mechanical loads, reducing stress concentration at any single point. This can lead to less initiation and propagation of cracks compared to stochastic structures, which might have irregularities and stress concentrators due to their random nature.

All samples tested at a maximum stress of 0.5 σ_y presented failure before 10^6 cycles, while the ones tested at a maximum stress of 0.1 σ_y showed high cycle fatigue resistance and infinite life close to a maximum stress of around 20 MPa, as shown in Figure 7. These results are similar to the ones obtained by Kelly *et al.* for close to 0.3 RD gyroid structures (Kelly *et al.*, 2019).

Figure 6 Gyroid vs stochastic dynamic assessment.

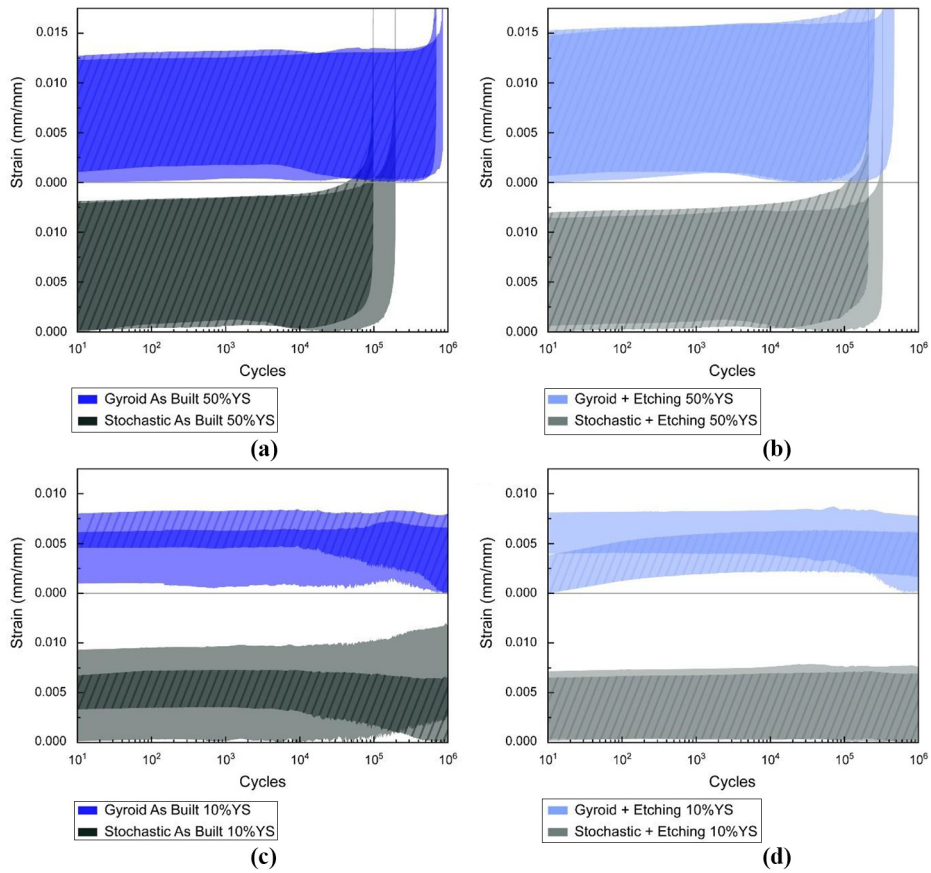

Notes: As built condition 0.5 σ_y (a) Etching treatment 0.5 σ_y; (b) As built condition 0.1 σ_y; (c) Etching treatment 0.1 σ_y; (d) The textured regions marked by lines indicate the strain range observed in a replicated fatigue test. The shaded area represents the overlap of strain ranges across multiple test runs
Source: Figure by authors

Figure 7 Compression–compression fatigue maximum stress of SLM Ti64 lattices with the variables: structure (Gyroid vs Stochastic), treatment (as-built vs etching) and force control (0.1 σ_y vs 0.5 σ_y)

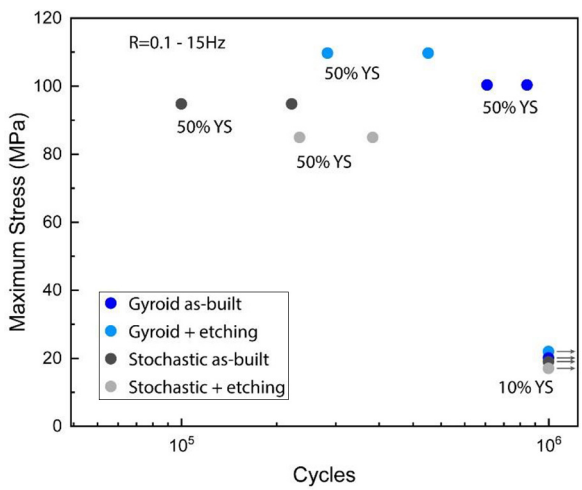

Source: Figure by authors

3.3 Failure analysis

Figure 8 presents the condition of the samples after fatigue testing. At 0.1 σ_y, the specimens did not present any significant and observable failure at the macro level. At 0.5 σ_y, the two structures and treatments presented a failure where shear bands at 45° can be observed. A 45° shear band is a typical mode of deformation for lattices produced by PBF-LB (Gorny *et al.*, 2011; Speirs *et al.*, 2017; Xiao *et al.*, 2019).

At a stress level corresponding to 0.1 σ_y, the observed lack of notable macroscopic failures indicates good resilience of the lattice structure under cyclic loading at lower stress levels, maintaining structural integrity without significant deformation or the initiation of cracks. This observation is consistent with the structures' behavior during static compression tests, where initial buckling did not lead to catastrophic failure, suggesting an inherent ability of the structures to absorb or redistribute stress below a certain intensity in the linear elastic regime. At a higher stress level of 0.5 σ_y, the predominant fatigue failure mechanism, characterized by the formation of 45° shear bands, mirrors the deformation pattern seen in static compression tests. This parallel indicates that under cyclic loading, the effects of stress concentration are magnified, promoting the initiation and subsequent propagation of fatigue cracks along these shear bands. This finding underscores the critical impact of cyclic stress amplitude on the fatigue life of lattice structures, highlighting the need for careful consideration of stress distribution and concentration effects in the design and application of such materials.

Figure 9 presents SEM images of both studied structures, subjected to the highest fatigue stress tested. The observed crack initiations leading to failure predominantly occurred at nodal points and the adjacent struts, consistent with previous observations of fatigue failure in metallic lattices (Speirs *et al.*, 2017; Wu *et al.*, 2017). This phenomenon is attributed to the redistribution of fatigue loading to the unit cell's connection nodes through the struts, resulting in significant stress concentration at their junctions (Wu *et al.*, 2017). The origins of fatigue cracks within the strut sections are primarily associated with surface irregularities rather than internal defects such as pores (Dallago *et al.*, 2018), as evidenced in Figure 9 (a), (d) and (k), .

The analyzed samples revealed distinct areas indicative of fatigue failure, characterized primarily by visible striations [Figure 9 (c), (f) and (l)] alongside zones of ductile failure [Figure 9(i)]. This dual-mode failure mechanism suggests a complex interaction between material properties and structural design in determining the fatigue life of AM components. Fatigue failure appears to be significantly influenced by fabrication defects related to scan parameters, which present as discontinuities of varying shapes and sizes within the walls and inconsistencies between perimeter and infill scan paths (Kelly *et al.*, 2019). AM process parameters were observed to be critical in defect formation, which in turn impacts the mechanical integrity and performance of printed metallic lattices.

3.4 In-vitro biocompatibility tests

The biocompatibility assays conducted at 48 and 72 h of incubation results for the SLM specimens are shown in Figure 10. The biocompatibility assays conducted at 48 and 72 h of incubation yielded positive results. A metallic material is considered biocompatible when the percentage of viable cells is equal to or higher than 70% (Assad and Jackson, 2019; Huzum *et al.*, 2021). The Alamar Blue assay results from the 48 h period show a strong cytocompatibility with cell survival rates of 76.4% for the SLM as-built samples and 92.0% for the SLM + Etching samples, affirming their biocompatibility. Furthermore, a notable improvement in cell viability was observed at the 72 h mark, with survival rates increasing to 79.5% for SLM as-built and reaching 105.7% for SLM + Etching, highlighting the potential of post-manufacturing treatments in enhancing biocompatibility.

The data presented shows no significant difference among cells growing over the specimen surface in SLM as built and SLM with etching at 48 h ($p = 0.264$), but higher viability of cells growing over the specimen surface in SLM + Etching specimens (56.7%) when compared to SLM as built (36.1%) at 72 h ($p = 0.016$). The higher viability of cells growing observed over the specimen surface in SLM + Etching suggests that the etching treatment holds promise for future use in medical devices since it allows cell growth better than as-built conditions upon longer incubation periods.

Approximately 45%–55% of the viable cells in the SLM treatments proliferate directly on the specimen surface after 48 and 72 h. This pattern indicates the presence of cell migration from the well surface toward the SLM specimen surface over the incubation time, or at least an increased proliferation from cells adhered to the specimens.

4. Conclusions

TPMS-gyroid and stochastic structures were successfully fabricated with relative densities ranging from 0.2 to 0.4. The as-built structures exhibited typical PBF-LB defects such as the staircase effect, voids and surface roughness. Etching significantly

Figure 8 Specimen after fatigue testing

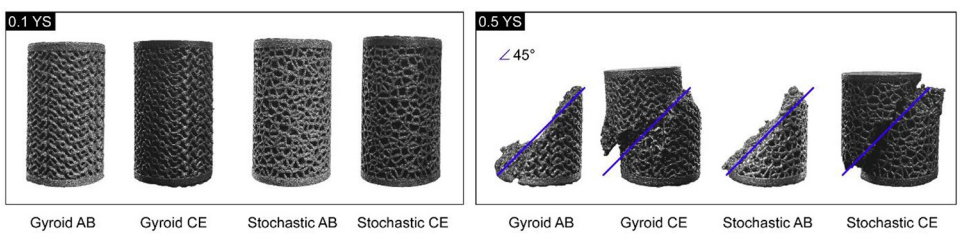

Source: Figure by authors

Figure 9 Micro-fractures SEM micrographs

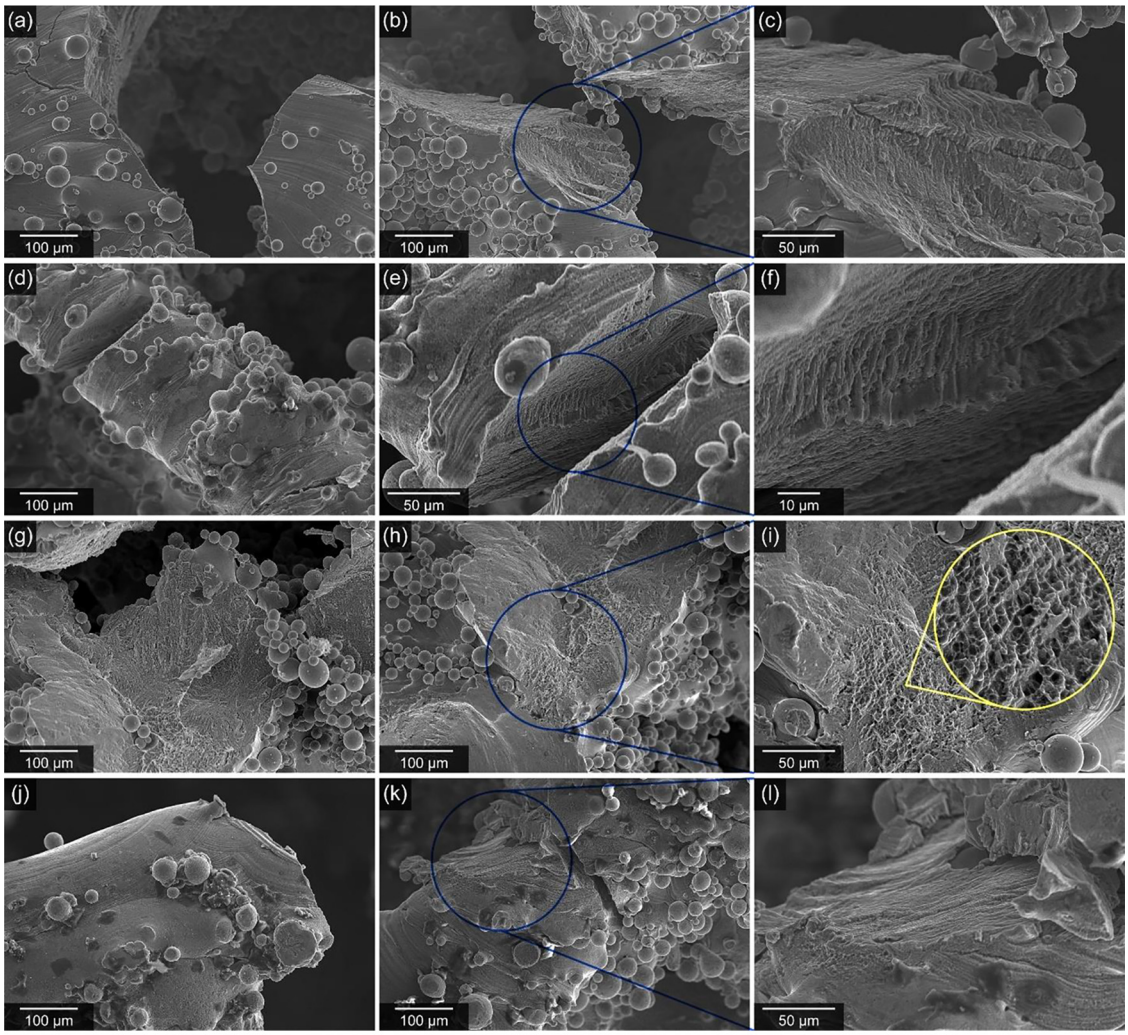

Notes: Gyroid as built (a,b,c), gyroid with chemical etching (d,e,f), stochastic as built (g, h, i) and stochastic with chemical etching (j,k,l)
Source: Figure by authors

Figure 10 Cell viability of SaOS-2 cell line growing in the surface of SLM specimens after 48 h (left) and 72 h (right) of direct contact

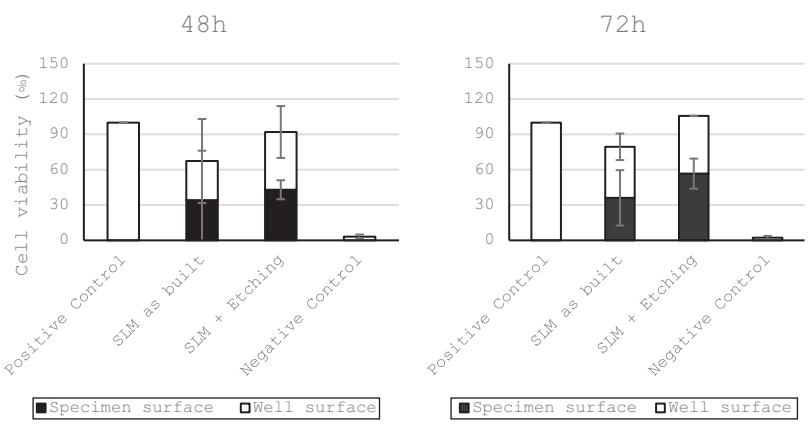

Source: Figure by authors

improved surface smoothness, potentially enhancing fatigue performance and biocompatibility.

The mechanical behavior of TPMS-Gyroid and Stochastic structures under static compressive loading reveals the critical role of geometry and post-processing in defining the material properties of Ti64 manufactured via PBF-LB. Specifically, the TPMS-Gyroid structures exhibited a progressive increase in Young's Modulus from 2.705 GPa at 0.2 RD to 4.580 GPa at 0.4 RD, and Yield Strength rose from 130.424 to 340.072 MPa in as-built conditions. Similarly, etched conditions showed improvements, with Young's Modulus increasing to 4.546 GPa and Yield Strength to 344.438 MPa at 0.4 RD. In contrast, Stochastic structures, while also showing increased mechanical properties with higher RD, generally had lower Young's Modulus and Yield Strength compared to the TPMS-Gyroid structures, with as-built conditions yielding a Young's Modulus ranging from 2.447 GPa at 0.2 RD to 4.361 GPa at 0.4 RD and Yield Strength from 111.426 to 259.093 MPa. These findings provide valuable insights for designing and manufacturing high-performance components in biomedical applications, where tailored mechanical properties are crucial. The mechanical characterization under static and dynamic loading conditions revealed that TPMS-gyroid and stochastic structures exhibit increased mechanical properties with higher relative densities. Etching generally improved these properties, especially in gyroid structures, likely due to the reduction of surface irregularities that act as stress concentrators. This improvement underscores the potential of etching as a beneficial post-manufacturing treatment for enhancing the fatigue performance of biomedical implants.

The fatigue behavior of Ti64 lattices was significantly influenced by the structural geometry (gyroid vs stochastic), surface treatment (as-built vs etching) and the level of applied stress (0.1 σ_y vs 0.5 σ_y). Stochastic structures offered more predictable and stable behavior under lower stress levels (0.1 σ_y), while Gyroid structures provided better high-cycle fatigue resistance under higher stress conditions (0.5 σ_y). The quantitative analysis reveals that both structures maintain stable strain amplitudes across as-built and etched conditions up to 10^5 cycles at 0.1 σ_y. Furthermore, etching has consistently been shown to improve fatigue resistance in both structures by maintaining or slightly increasing the strain amplitude over cycles., likely by removing surface defects and reducing stress concentrators, though its benefits are more pronounced at lower stress levels This is demonstrated in the sustained performance of samples under a maximum stress of 0.1 σ_y, which exhibited high cycle fatigue resistance and an effective infinite life close to a stress threshold of around 20 MPa.

In-vitro biocompatibility tests indicated that both as-built and etched samples are biocompatible, with etched samples showing a significant improvement in cell viability after 72 h of incubation. This suggests that etching not only enhances mechanical properties but also has a positive impact on the biocompatibility of Ti64 lattice structures, making them promising candidates for biomedical applications.

The results of this study highlight the potential of using etched TPMS-gyroid and stochastic Ti64 structures fabricated via PBF-LB in biomedical applications, particularly for implants requiring high fatigue resistance and biocompatibility. The ability to tailor mechanical properties through design and post-processing treatments presents a valuable approach to optimizing implant performance according to specific application needs. Further research is encouraged to explore the long-term biocompatibility and in-vivo performance of these structures and develop more efficient and environmentally friendly etching processes that could enhance the mechanical properties and biocompatibility of Ti64 components for medical use.

References

Ahmadi, S.M., Kumar, R., Borisov, E.V., Petrov, R., Leeflang, S., Li, Y., Tümer, N., Huizenga, R., Ayas, C., Zadpoor, A.A. and Popovich, V.A. (2019), "From microstructural design to surface engineering: a tailored approach for improving fatigue life of additively manufactured meta-biomaterials", *Acta Biomaterialia*, Vol. 83, pp. 153-166, doi: 10.1016/j.actbio.2018.10.043.

Araya, M., Jaskari, M., Rautio, T., Guillén, T. and Järvenpää, A. (2024), "Assessing the compressive and tensile properties of TPMS-Gyroid and stochastic Ti64 lattice structures: a study on laser powder bed fusion manufacturing for biomedical implants", *Journal of Science: Advanced Materials and Devices*, Vol. 9 No. 1, p. 100663, doi: 10.1016/j.jsamd.2023.100663.

Ashby, M.F. and Medalist, R.F.M. (1983), "The mechanical properties of cellular solids", *Metallurgical Transactions A*, Vol. 14 No. 9, pp. 1755-1769, doi: 10.1007/BF02645546.

Assad, M. and Jackson, N. (2019), "Biocompatibility evaluation of orthopedic biomaterials and medical devices: a review of safety and efficacy models", *Encyclopedia of Biomedical Engineering*, pp. 281-309, doi: 10.1016/B978-0-12-801238-3.11104-3.

Ataee, A., Li, Y., Fraser, D., Song, G. and Wen, C. (2018), "Anisotropic Ti-6Al-4V gyroid scaffolds manufactured by electron beam melting (EBM) for bone implant applications", *Materials & Design*, Vol. 137, pp. 345-354, doi: 10.1016/j.matdes.2017.10.040.

Bandyopadhyay, A., Mitra, I., Goodman, S.B., Kumar, M. and Bose, S. (2023), "Improving biocompatibility for next generation of metallic implants", *Progress in Materials Science*, Vol. 133, p. 101053, doi: 10.1016/j.pmatsci.2022.101053.

Barba, D., Alabort, E. and Reed, R.C. (2019), "Synthetic bone: design by additive manufacturing", *Acta Biomaterialia*, Vol. 97, pp. 637-656, doi: 10.1016/j.actbio.2019.07.049.

Bartolomeu, F., Costa, M.M., Alves, N., Miranda, G. and Silva, F.S. (2021), "Selective laser melting of Ti6Al4V Sub-millimetric cellular structures: prediction of dimensional deviations and mechanical performance", *Journal of the Mechanical Behavior of Biomedical Materials*, Vol. 113, p. 104123, doi: 10.1016/j.jmbbm.2020.104123.

Bobbert, F.S.L., Lietaert, K., Eftekhari, A.A., Pouran, B., Ahmadi, S.M., Weinans, H. and Zadpoor, A.A. (2017), "Additively manufactured metallic porous biomaterials based on minimal surfaces: a unique combination of topological, mechanical, and mass transport properties", *Acta Biomaterialia*, Vol. 53, pp. 572-584, doi: 10.1016/j.actbio.2017.02.024.

Bregoli, C., Fiocchi, J., Biffi, C.A. and Tuissi, A. (2024), "Additively manufactured medical bone screws: an initial study to investigate the impact of lattice-based voronoi structure on

implant primary stability", *Rapid Prototyping Journal*, Vol. 30 No. 1, pp. 60-72, doi: 10.1108/RPJ-10-2022-0363.

Cao, X., Carter, L.N., Villapún, V.M., Cantaboni, F., De Sio, G., Lowther, M., Louth, S.E.T., *et al.* (2022), "Optimisation of single contour strategy in selective laser melting of Ti-6Al-4V lattices", *Rapid Prototyping Journal*, Vol. 28 No. 5, pp. 907-915, doi: 10.1108/RPJ-04-2021-0103.

Choy, S.Y., Sun, C.-N., Leong, K.F. and Wei, J. (2017), "Compressive properties of Ti-6Al-4V lattice structures fabricated by selective laser melting: design, orientation and density", *Additive Manufacturing*, Vol. 16, pp. 213-224, doi: 10.1016/j.addma.2017.06.012.

Claros, C.A.E., Oliveira, D.P., Campanelli, L.C., Pereira da Silva, P.S.C. and Bolfarini, C. (2016), "Fatigue behavior of Ti–6Al–4V alloy in saline solution with the surface modified at a micro- and nanoscale by chemical treatment", *Materials Science and Engineering: C*, Vol. 67, pp. 425-432, doi: 10.1016/j.msec.2016.04.099.

Dallago, M., Fontanari, V., Torresani, E., Leoni, M., Pederzolli, C., Potrich, C. and Benedetti, M. (2018), "Fatigue and biological properties of Ti-6Al-4V ELI cellular structures with variously arranged cubic cells made by selective laser melting", *Journal of the Mechanical Behavior of Biomedical Materials*, Vol. 78, pp. 381-394, doi: 10.1016/j.jmbbm.2017.11.044.

Deering, J. and Grandfield, K. (2021), "Current interpretations on the in vivo response of bone to additively manufactured metallic porous scaffolds: a review", *Biomaterials and Biosystems*, Vol. 2, p. 100013, doi: 10.1016/j.bbiosy.2021.100013.

Dhiman, S., Sidhu, S.S., Bains, P.S. and Bahraminasab, M. (2019), "Mechanobiological assessment of Ti-6Al-4V fabricated via selective laser melting technique: a review", *Rapid Prototyping Journal*, Vol. 25 No. 7, pp. 1266-1284, doi: 10.1108/RPJ-03-2019-0057.

Evans, S., Jones, E., Fox, P. and Sutcliffe, C. (2018), "Photogrammetric analysis of additive manufactured metallic open cell porous structures", *Rapid Prototyping Journal*, Vol. 24 No. 8, pp. 1380-1391, doi: 10.1108/RPJ-05-2017-0082.

Ghouse, S., Babu, S., Nai, K., Hooper, P.A. and Jeffers, J.R.T. (2018), "The influence of laser parameters, scanning strategies and material on the fatigue strength of a stochastic porous structure", *Additive Manufacturing*, Vol. 22, pp. 290-301, doi: 10.1016/j.addma.2018.05.024.

Ghouse, S., Babu, S., Van Arkel, R.J., Nai, K., Hooper, P.A. and Jeffers, J.R.T. (2017), "The influence of laser parameters and scanning strategies on the mechanical properties of a stochastic porous material", *Materials & Design*, Vol. 131, pp. 498-508, doi: 10.1016/j.matdes.2017.06.041.

Gibson, L.J. (2005), "Biomechanics of cellular solids", *Journal of Biomechanics*, Vol. 38 No. 3, pp. 377-399, doi: 10.1016/j.jbiomech.2004.09.027.

Gorny, B., Niendorf, T., Lackmann, J., Thoene, M., Troester, T. and Maier, H.J. (2011), "In situ characterization of the deformation and failure behavior of non-stochastic porous structures processed by selective laser melting", *Materials Science and Engineering: A*, Vol. 528 No. 27, pp. 7962-7967, doi: 10.1016/j.msea.2011.07.026.

Günther, F., Pilz, S., Hirsch, F., Wagner, M., Kästner, M., Gebert, A. and Zimmermann, M. (2023), "Shape optimization of additively manufactured lattices based on triply periodic minimal surfaces", *Additive Manufacturing*, Vol. 73, p. 103659, doi: 10.1016/j.addma.2023.103659.

Hanks, B., Berthel, J., Frecker, M. and Simpson, T.W. (2020), "Mechanical properties of additively manufactured metal lattice structures: data review and design interface", *Additive Manufacturing*, Vol. 35, p. 101301, doi: 10.1016/j.addma.2020.101301.

Huang, X., Lang, L., Gong, S. and Zhao, M. (2020), "Effect of post-treatment on the microstructure and mechanical properties of selective laser melted Ti6Al4V lattice structures", *Rapid Prototyping Journal*, Vol. 26 No. 9, pp. 1569-1577, doi: 10.1108/RPJ-11-2019-0284.

Huang, H., Wang, L. and Fan, Y. (2023), "Metallic meta-biomaterials: a critical review of fatigue behaviors", *Journal of Science: Advanced Materials and Devices*, Vol. 8 No. 3, p. 100585, doi: 10.1016/j.jsamd.2023.100585.

Huzum, B., Puha, B., Necoara, R., Gheorghevici, S., Puha, G., Filip, A., Sirbu, P. (2021), "Biocompatibility assessment of biomaterials used in orthopedic devices: an overview (review)", *Experimental and Therapeutic Medicine*, Vol. 22 No. 5, p. 1315, doi: 10.3892/etm.2021.10750.

Jam, A., Du Plessis, A., Lora, C., Raghavendra, S., Pellizzari, M. and Benedetti, M. (2022), "Manufacturability of lattice structures fabricated by laser powder bed fusion: a novel biomedical application of the beta Ti-21S alloy", *Additive Manufacturing*, Vol. 50, p. 102556, doi: 10.1016/j.addma.2021.102556.

Karami, K., Blok, A., Weber, L., Ahmadi, S.M., Petrov, R., Nikolic, K., Borisov, E.V., Leeflang, S., Ayas, C., Zadpoor, A.A. and Mehdipour, M. (2020), "Continuous and pulsed selective laser melting of Ti6Al4V lattice structures: effect of post-processing on microstructural anisotropy and fatigue behaviour", *Additive Manufacturing*, Vol. 36, p. 101433, doi: 10.1016/j.addma.2020.101433.

Kechagias, S., Oosterbeek, R.N., Munford, M.J., Ghouse, S. and Jeffers, J.R.T. (2022), "Controlling the mechanical behaviour of stochastic lattice structures: the key role of nodal connectivity", *Additive Manufacturing*, Vol. 54, p. 102730, doi: 10.1016/j.addma.2022.102730.

Kelly, C.N., Francovich, J., Julmi, S., Safranski, D., Guldberg, R.E., Maier, H.J. and Gall, K. (2019), "Fatigue behavior of as-built selective laser melted titanium scaffolds with sheet-based gyroid microarchitecture for bone tissue engineering", *Acta Biomaterialia*, Vol. 94, pp. 610-626, doi: 10.1016/j.actbio.2019.05.046.

Kumawat, S., Deshmukh, S.R. and Ghorpade, R.R. (2023), "Fabrication of Ti-6Al-4v cellular lattice structure using selective laser melting for orthopedic use: a review", *Materials Today: Proceedings*, doi: 10.1016/j.matpr.2023.08.053.

McGregor, M., Patel, S., McLachlin, S. and Vlasea, M. (2021), "Architectural bone parameters and the relationship to titanium lattice design for powder bed fusion additive manufacturing", *Additive Manufacturing*, Vol. 47, p. 102273, doi: 10.1016/j.addma.2021.102273.

Ma, S., Tang, Q., Han, X., Feng, Q., Song, J., Setchi, R., Liu, Y., Liu, Y., Goulas, A., Engstrøm, D.S. and Tse, Y.Y. (2020), "Manufacturability, mechanical properties, Mass-Transport properties and biocompatibility of triply periodic minimal surface (TPMS) porous scaffolds fabricated by

selective laser melting", *Materials & Design*, Vol. 195, p. 109034, doi: 10.1016/j.matdes.2020.109034.

Marin, E. (2023), "Forged to heal: the role of metallic cellular solids in bone tissue engineering", *Materials Today Bio*, Vol. 23, p. 100777, doi: 10.1016/j.mtbio.2023.100777.

Mondal, P., Das, A., Wazeer, A. and Karmakar, A. (2022), "Biomedical porous scaffold fabrication using additive manufacturing technique: porosity, surface roughness and process parameters optimization", *International Journal of Lightweight Materials and Manufacture*, Vol. 5 No. 3, pp. 384-396, doi: 10.1016/j.ijlmm.2022.04.005.

Murr, L.E., Amato, K.N., Li, S.J., Tian, Y.X., Cheng, X.Y., Gaytan, S.M., Martinez, E. (2011), "Microstructure and mechanical properties of open-cellular biomaterials prototypes for total knee replacement implants fabricated by electron beam melting", *Journal of the Mechanical Behavior of Biomedical Materials*, Vol. 4 No. 7, pp. 1396-1411, doi: 10.1016/j.jmbbm.2011.05.010.

Oosterbeek, R.N., Sirbu, G., Hansal, S., Nai, K. and Jeffers, J. R.T. (2023), "Effect of chemical–electrochemical surface treatment on the roughness and fatigue performance of porous titanium lattice structures", *Additive Manufacturing*, Vol. 78, p. 103896, doi: 10.1016/j.addma.2023.103896.

Pereira, H., Cengiz, I.F., Maia, F.R., Bartolomeu, F., Oliveira, J.M., Reis, R.L. and Silva, F.S. (2020), "Physicochemical properties and cytocompatibility assessment of non-degradable scaffolds for bone tissue engineering applications", *Journal of the Mechanical Behavior of Biomedical Materials*, Vol. 112, p. 103997, doi: 10.1016/j.jmbbm.2020.103997.

Seharing, A., Azman, A.H. and Abdullah, S. (2020), "Finite element analysis of gradient lattice structure patterns for bone implant design", *International Journal of Structural Integrity*, Vol. 11 No. 4, pp. 535-545, doi: 10.1108/IJSI-03-2020-0028.

Soro, N., Brodie, E.G., Abdal-Hay, A., Alali, A.Q., Kent, D. and Dargusch, M.S. (2022), "Additive manufacturing of biomimetic Titanium-Tantalum lattices for biomedical implant applications", *Materials & Design*, Vol. 218, p. 110688, doi: 10.1016/j.matdes.2022.110688.

Speirs, M., Van Hooreweder, B., Van Humbeeck, J. and Kruth, J.-P. (2017), "Fatigue behaviour of NiTi shape memory alloy scaffolds produced by SLM, a unit cell design comparison", *Journal of the Mechanical Behavior of Biomedical Materials*, Vol. 70, pp. 53-59, doi: 10.1016/j.jmbbm.2017.01.016.

Sun, Q., Sun, J., Guo, K. and Wang, L. (2022), "Compressive mechanical properties and energy absorption characteristics of SLM fabricated Ti6Al4V triply periodic minimal surface cellular structures", *Mechanics of Materials*, Vol. 166, p. 104241, doi: 10.1016/j.mechmat.2022.104241.

Sun, Y.Y., Lu, S.L., Gulizia, S., Oh, C.H., Fraser, D., Leary, M. and Qian, M. (2020), "Fatigue performance of additively manufactured Ti-6Al-4V: surface condition vs. Internal defects", *JOM*, Vol. 72 No. 3, pp. 1022-1030, doi: 10.1007/s11837-020-04025-7.

Surmeneva, M.A., Khrapov, D., Prosolov, K., Kozadayeva, M., Koptyug, A., Volkova, A., Paveleva, A. and Surmenev, R.A. (2022), "The influence of chemical etching on porous structure and mechanical properties of the Ti6AL4V functionally graded porous scaffolds fabricated by EBM", *Materials Chemistry and Physics*, Vol. 275, p. 125217, doi: 10.1016/j.matchemphys.2021.125217.

Tan, X.P., Tan, Y.J., Chow, C.S.L., Tor, S.B. and Yeong, W.Y. (2017), "Metallic powder-bed based 3D printing of cellular scaffolds for orthopaedic implants: a state-of-the-art review on manufacturing, topological design, mechanical properties and biocompatibility", *Materials Science and Engineering: C*, Vol. 76, pp. 1328-1343, doi: 10.1016/j.msec.2017.02.094.

Timercan, A., Terriault, P. and Brailovski, V. (2023), "Axial tension/compression and torsional loading of diamond and gyroid lattice structures for biomedical implants: simulation and experiment", *Materials & Design*, Vol. 225, p. 111585, doi: 10.1016/j.matdes.2022.111585.

Tyagi, S.A. and Manjaiah, M. (2023), "Additive manufacturing of titanium-based lattice structures for medical applications – a review", *Bioprinting*, Vol. 30, p. e00267, doi: 10.1016/j.bprint.2023.e00267.

Van Hooreweder, B. and Kruth, J.-P. (2017), "Advanced fatigue analysis of metal lattice structures produced by selective laser melting", *CIRP Annals*, Vol. 66 No. 1, pp. 221-224, doi: 10.1016/j.cirp.2017.04.130.

Van Hooreweder, B., Apers, Y., Lietaert, K. and Kruth, J.-P. (2017), "Improving the fatigue performance of porous metallic biomaterials produced by selective laser melting", *Acta Biomaterialia*, Vol. 47, pp. 193-202, doi: 10.1016/j.actbio.2016.10.005.

Vyavahare, S., Mahesh, V., Mahesh, V. and Harursampath, D. (2023), "Additively manufactured meta-biomaterials: a state-of-the-art review", *Composite Structures*, Vol. 305, p. 116491, doi: 10.1016/j.compstruct.2022.116491.

Wu, M.-W., Chen, J.-K., Lin, B.-H. and Chiang, P.-H. (2017), "Improved fatigue endurance ratio of additive manufactured Ti-6Al-4V lattice by hot isostatic pressing", *Materials & Design*, Vol. 134, pp. 163-170, doi: 10.1016/j.matdes.2017.08.048.

Wu, Y., Liu, J., Kang, L., Tian, J., Zhang, X., Hu, J., Huang, Y., Liu, F., Wang, H. and Wu, Z. (2023), "An overview of 3D printed metal implants in orthopedic applications: present and future perspectives", *Heliyon*, Vol. 9 No. 7, p. e17718, doi: 10.1016/j.heliyon.2023.e17718.

Xiao, L., Song, W., Hu, M. and Li, P. (2019), "Compressive properties and micro-structural characteristics of Ti–6Al–4V fabricated by electron beam melting and selective laser melting", *Materials Science and Engineering: A*, Vol. 764, p. 138204, doi: 10.1016/j.msea.2019.138204.

Yan, X., Li, Q., Yin, S., Chen, Z., Jenkins, R., Chen, C., Wang, J., Ma, W., Bolot, R., Lupoi, R. and Ren, Z. (2019), "Mechanical and in vitro study of an isotropic Ti6Al4V lattice structure fabricated using selective laser melting", *Journal of Alloys and Compounds*, Vol. 782, pp. 209-223, doi: 10.1016/j.jallcom.2018.12.220.

Yang, L., Mertens, R., Ferrucci, M., Yan, C., Shi, Y. and Yang, S. (2019), "Continuous graded gyroid cellular structures fabricated by selective laser melting: design, manufacturing and mechanical properties", *Materials & Design*, Vol. 162, pp. 394-404, doi: 10.1016/j.matdes.2018.12.007.

Yu, G., Li, X., Dai, L., Xiao, L. and Song, W. (2022), "Compressive properties of imperfect Ti-6Al-4V lattice structure fabricated by electron beam powder bed fusion under static and dynamic loadings", *Additive Manufacturing*, Vol. 49, p. 102497, doi: 10.1016/j.addma.2021.102497.

Zhang, C., Qiao, H., Yang, L., Ouyang, W., He, T., Liu, B., Chen, X., Wang, N. and Yan, C. (2024), "Vibration characteristics of additive manufactured IWP-type TPMS lattice structures", *Composite Structures*, Vol. 327, p. 117642, doi: 10.1016/j.compstruct.2023.117642.

Zhao, D., Liang, H., Han, C., Li, J., Liu, J., Zhou, K., Yang, C. and Wei, Q. (2021), "3D printing of a titanium-tantalum gyroid scaffold with superb elastic admissible strain, bioactivity and in-situ bone regeneration capability", *Additive Manufacturing*, Vol. 47, p. 102223, doi: 10.1016/j.addma.2021.102223.

Corresponding author

Miguel Araya-Calvo can be contacted at: miaraya@itcr.ac.cr